Models for DNA Backbone Motions: An Interpretation of NMR Relaxation Experiments

Joe W. Keepers* and Thomas L. James[1]

Contribution from the Department of Pharmaceutical Chemistry, University of California, San Francisco, California 94143. *Received May 12, 1981*

Abstract: To elucidate the motions in double helical nucleic acids which may be responsible for the observed ^{31}P and ^{13}C NMR relaxation properties, the theory and mathematical models have been developed for these motions. Using autocorrelation functions constructed from the motional models, the spin-lattice relaxation times (T_1), the nuclear Overhauser effect (NOE), and the line widths appropriate for comparison with the experimental ^{31}P and ^{13}C data of the DNA backbone were calculated. Although the relaxation of protonated ^{13}C nuclei could be treated as solely dipolar in origin, it was necessary to include contributions from the chemical shift anisotropy (CSA) as well as the dipolar contributions from the H3′, H5′, and H5″ protons for ^{31}P relaxation. Since the P-H dipolar vectors fluctuate in distance and orientation with the molecular motions, the theory to explicitly account for these fluctuations was developed. Variations of two different jump models were examined. The first class of models considers the reorientation of the ^{31}P CSA tensor, P-H dipolar vectors (as well as P-H distance fluctuations), and C-H dipolar vectors relative to the helix axis as a reference frame. This class of models is useful for investigating concerted motions, for example, reorientation of the torsional angles of the six backbone bonds in each monomeric unit of a polynucleotide. This model is used to calculate the backbone NMR relaxation parameter values expected from DNA winding and unwinding motions (torsional twist), base tilting motions, and base propeller twisting motions. A second class of models utilizes the deoxyribose ring in DNA as the frame of reference for any internal motions. The influence of conformational fluctuations in the deoxyribose ring (puckering motions) on ^{31}P and ^{13}C relaxation could be examined using a jump axis which intersects either C1′ or C4′ and bisects the C2′-C3′ bond. Some variants of this basic model add rotational jumps about the various bonds in the phosphodiester moiety of the backbone as well. Comparison of experimental ^{13}C and ^{31}P relaxation data for atoms along the backbone and in the sugar ring of DNA with the results calculated using the various motional models revealed the following. (a) Explicitly accounting for the P-H distance fluctuations is essential for understanding the ^{31}P data when the CSA contribution is also considered. (b) The DNA winding and unwinding, base tilting, and base-pair propeller twisting motions have little effect on NMR relaxation. (c) The ^{13}C relaxation of ring carbons can be accounted for by sugar repuckering jumps; the ^{13}C relaxation of C5′ and the ^{31}P relaxation are consistent with the sugar repucker model with additional rotational jumps about the C4′-C5′ bond or C3′-O3′ bond and the O3′-P (or O5′-P) bonds. The best fit to the experimental data was obtained with a motional model having a sugar repucker rotational jump of 70°, C4′-C5′ (and O3′-C3′) bond rotational jump of 50°, and O3′-P and P-O5′ rotational jumps for 50°. The correlation times for each of these motions is subnanosecond.

Introduction

Deoxyribonucleic acid (DNA) exhibits several types of conformational fluctuations occurring in the frequency range 10^6 to 10^{12} s^{-1}. These fluctuations have been an increasing area of interest because of their importance in recognition and transcription events as well as protein and drug-nucleic acid interactions.[2] This flexibility has been described as arising from breathing motions, kinking, and the smooth deformations resulting from DNA's behavior as a worm-like coil. For studying the amplitudes and frequencies of these motions they may be conveniently classified as motions which reorient (1) the whole polymer (overall motion), (2) large segments of the polymer (segmental motion), or (3) the atoms in the nucleotide units within the biopolymer (internal motions).

Nuclear magnetic resonance (NMR) relaxation experiments may be used to monitor the magnetic fluctuations arising from the overall, segmental, and internal motions of DNA, and these studies have been used to characterize the frequency and amplitudes of these motions within the mathematical model(s), relating them to the magnetic fluctuations measured by the NMR experiment.[3] Additional information with regard to frequency and amplitude motional parameters may be obtained from other spectroscopic techniques; for example, fluorescence depolarization of intercalated ethidium has been used to examine the conformational fluctuations occurring in DNA.[4] A correlation function based upon the elastic properties of double helical DNA was developed for the interpretation of the fluorescence depolarization of the intercalator ethidium bromide.[5] The molecular geometry of double helical DNA places constraints upon its elastic properties, and these constraints have recently been included in calculations reproducing the experimental equilibrium hydrodynamic properties of DNA.[6] In contrast to fluorescence depolarization or hydrodynamic experiments, NMR relaxation experiments are most sensitive to the local fluctuations (internal motions) in these polymers; however, full advantage of the constraints placed upon these motions by the molecular geometry of the system, particularly in the case of double helical structures, has not been utilized in interpretating the NMR relaxation data.

In addition to the information provided by the molecular geometry, the constraints placed upon the frequency and amplitude of possible motions in nucleic acid may also be characterized from the relaxation experiments by a detailed analysis of the contributing NMR relaxation mechanisms. For example, it may be the case that both the dipole-dipole (DD) and chemical shift anisotropy (CSA) mechanisms make a significant contribution to the relaxation process of ^{31}P nuclei within the backbone of the polynucleotides. While complicating the procedure for extracting detailed motional information from the relaxation data, two

(1) Recipient of Research Career Development Award AM00291 from NIH.

(2) (a) Sarma, R. H., Ed. "Nucleic Acid Geometry and Dynamics"; Pergamon: New York, 1961. (b) Wells, R. D.; Goodman, T. C.; Hillen, W.; Horn, G. T.; Klein, R. D.; Larson, J. E.; Muller, U. R.; Neuendorf, S. K.; Panayotatos, N.; Stirdivant, S. M. *Prog. Nucleic Acid Res. Mol. Biol.* **1980**, *24*, 167-265.

(3) James, T. L. *Bull. Magn. Reson.*, in press.

(4) (a) Wahl, P.; Paoletti, P.; Le Pecq, J. B. *Proc. Natl. Acad. Sci. USA* **1970**, *65*, 417-421. (b) Genest, D.; Wahl, P. *Biochim. Biophys. Acta* **1978**, *521*, 502-509. (c) Thomas, J. C.; Allison, S. A.; Appellof, C. J.; Schurr, M. J. *Biophys. Chem.* **1980**, *12*, 177-188. (d) Millar, D. P.; Robbins, R. J.; Zewail, A. H. *Proc. Natl. Acad. Sci., USA*, **1980**, *77*, 5593-5597.

(5) (a) Barkley, M. D.; Zimm, B. H. *J. Chem. Phys.* **1979**, *70*, 2991-3007. (b) Allison, S. A.; Schurr, J. M. *Chem. Phys.* **1979**, *41*, 35-59.

(6) (a) Olson, W. K. *Biopolymers* **1976**, *15*, 859-878. (b) Olson, W. K. *Ibid.* **1979**, *18*, 1213-1233. (c) Olson, W. K. *Ibid.* **1979**, *18*, 1235-1260. (d) Olson, W. K. *Macromolecules* **1980**, *13*, 721-728. (e) Schellman, J. A. *Biopolymers* **1974**, *13*, 217-226. (f) Schellman, J. A. *Biophys. Chem.* **1980**, *11*, 329-377. (g) Schellman, J. A. *Ibid.* **1980**, *11*, 321-328.

0002-7863/82/1504-0929$01.25/0

contributing relaxation mechanisms may provide the complementary information necessary to test for a given set of internal motions. Models of the dipole–dipole contribution to the relaxation of protonated ^{13}C nuclei are well developed; however, the dipole–dipole relaxation contribution for phosphorus is less developed because of the additional complication imposed by the dipolar interaction with nuclei (typically hydrogen) removed by more than two bonds. In contrast to the usual ^{13}C case, the magnitude as well as the relative orientation of the dipole vector connecting the two interacting spins changes with and is coupled to the internal rotation. Typically authors have used an average distance and orientation in determining the dipole–dipole contribution to the ^{31}P relaxation times. The contribution of the "other" relaxation mechanism is then estimated from this result.

In this paper we develop the theory necessary to explicitly account for the fluctuations in both the magnitude and orientation of the dipolar coupling vectors (i.e., P–H) for the backbone phosphorus atoms in a DNA which is subject to internal motions of the six backbone bonds separating base pairs.[7] To apply this theory it is only necessary that a jump model appropriately treat the internal motion(s) which changes the magnitude of the dipole–dipole vector (i.e., P–H). Several studies of phosphorus nuclear magnetic relaxation in polynucleotides have appeared.[8] Depending on the length of the polynucleotide, the overall motion has been modeled as isotropic, or as the cylindrically anisotropic motion of a rigid rod.[8] The six internal motions have been treated either as a single free diffusion or two-state jump. However, none of these models explicitly included the fluctuations in magnitude of the ^{31}P–H3′, -H5′, and -H5″ dipolar vectors.

Second, we use this theory to examine several variations of two basic rotational jump models relating the internal motions to the structure of double helical DNA. The first model assumes that the reference segment subject to the overall or segmental motion is defined by the helix axis. In the context of this motional model, we examine the possible contributions of winding and unwinding motions, of base tilting motions, and of base twisting motions on the NMR relaxation of ^{31}P and the ^{13}C in the deoxyribose moiety. The second model assumes that the reference segment is the deoxyribose sugar unit and is defined by a jump axis bisecting the C2′–C3′ bond and intersecting C1′ or C4′. This particular model permits an examination of the influence of coformational fluctuations in the deoxyribose ring on the ^{13}C and ^{31}P relaxation processes. Some of the variations in this basic model entail rotational jumps about the various bonds in the phosphodiester moiety of the backbone in addition. The predictions of the models are compared with available data and with the models previously used to interpret the data.

Theory

While both the DD and CSA mechanisms may contribute to phosphorus relaxation in DNA, the ^{13}C relaxation for the deoxyribose carbons is dominated by the DD mechanism due to directly bonded protons. The Hamiltonian for these mechanisms may be written as the product of two spherical tensors,

$$\mathcal{H} = \sum_q (-)^q F_q A_{-q} \tag{1}$$

where A_q is a function of the spin operators and F_q are the familiar orientation factors or second-order spherical harmonics. For both the DD and CSA mechanisms the time dependence is contained entirely in the orientation factors.[9] The autocorrelation functions for the F_q are constructed from motional models, as shown below. The spin–lattice relaxation time, T_1, line width, $(\pi T_2)^{-1}$, and nuclear Overhauser effect, NOE, are computed from the Fourier transform of the autocorrelation function, i.e., the spectral densities $J(\omega)$ where

$$J(\omega) = 2\int_0^\infty \langle F_q(\Omega,0)F_q^*(\Omega,t)\rangle \cos(\omega t)\, dt \tag{2}$$

Ω represents the Euler angles (α, β, γ), which specify the orientation of the DD vector or the principal axis system (PAS) of the CSA tensor at a time 0 and some later time t, respectively, relative to the reference frame of the magnetic field. The relaxation parameters for the DD and CSA mechanisms are written as functions of the spectral densities and given by eq 3–10.

$$T_{1DD}^{-1} = \frac{3}{20}\gamma_{p,c}^2\gamma_h^2\hbar^2\sum_1^n [J(\omega_{p,c}-\omega_h) + 3J(\omega_{p,c}) + 6J(\omega_{p,c}+\omega_h)] \tag{3}$$

$$(\pi T_{2DD})^{-1} = \frac{3}{40\pi}\gamma_{p,c}^2\gamma_h^2\hbar^2 \times \sum_1^n [4J(0) + 6J(\omega_h) + J(\omega_{p,c}-\omega_h) + 3J(\omega_{p,c}) + 6J(\omega_{p,c}+\omega_h)] \tag{4}$$

$$NOE_{DD} = 1 + \frac{\gamma_h}{\gamma_{p,c}}\sum_1^n \frac{[6J(\omega_{p,c}+\omega_h) - J(\omega_{p,c}-\omega_h)]}{[J(\omega_{p,c}-\omega_h) + 3J(\omega_{p,c}) + 6J(\omega_{p,c}+\omega_h)]} \tag{5}$$

$$T_{1CSA}^{-1} = \frac{1}{15}\gamma_p^2 H_0^2 \Delta\sigma^2 J(\omega_p) \tag{6}$$

$$(\pi T_{2CSA})^{-1} = {}^1/_{90}\gamma_p^2 H_0^2 \Delta\sigma^2 [4J(0) + 3J(\omega_p)] \tag{7}$$

$$T_1^{-1} = T_{1DD}^{-1} + T_{1CSA}^{-1} \tag{8}$$

$$(\pi T_2)^{-1} = (\pi T_{2DD})^{-1} + (\pi T_{2CSA})^{-1} \tag{9}$$

$$NOE = 1 + (\gamma_h/\gamma_{p,c})\{({}^3/_{20}\gamma_{p,c}^2\gamma_h^2\hbar^2\sum_1^n [6J(\omega_{p,c}+\omega_h) - J(\omega_{p,c}-\omega_h)])/({}^3/_{20}\gamma_{p,c}^2\gamma_h^2\hbar^2\sum_1^n [J(\omega_{p,c}-\omega_h) + 3J(\omega_{p,c}) + 6J(\omega_{p,c}+\omega_h)] + T_{1CSA}^{-1})\} \tag{10}$$

$$\Delta\sigma = \sigma_{33} - {}^1/_2(\sigma_{11} + \sigma_{22}) \tag{11}$$

$$\delta_{ii} = \sigma_{ii} - {}^1/_3(\sigma_{11} + \sigma_{22} + \sigma_{33}) \tag{12}$$

$$\eta = (\delta_x - \delta_y)/\delta_z \tag{13}$$

In the dipolar expressions, $\omega_{p,c,h}$ refers to ^{31}P, ^{13}C, or ^1H Larmor frequency, whichever is appropriate, while $\gamma_{p,c,h}$ are the respective gyromagnetic ratios. The summations in eq 3–5, 10 are over the n hydrogen atoms dipolar coupled to a ^{31}P or ^{13}C nucleus. The dipolar equations are in a slightly modified form from those usually given because the dependence of the DD contribution on internuclear distances is included explicitly in the calculation of the autocorrelation function. This is necessary (as shown below) because the ^{31}P–H internuclear distance is a time-dependent function of the internal motions. The dependence of the CSA contribution on the magnetic field strength, H_0 and diagonal components of the CSA tensor $\Delta\sigma$ is evident from the equations.

Correlation Functions and Spectral Densities. The angular autocorrelation function $G(\tau)$ from which the spectral density functions are calculated may be written in terms of the Wigner rotation matrices, D_{lm}[10] (eq 14 and 15).

$$G(\tau)_{DD} = \langle F_q(\Omega,0)F_q^*(\Omega,t)\rangle = \langle D_{q0}^*(\alpha_{LF},\beta_{LF},\gamma_{LF};0)D_{q0}(\alpha_{LF},\beta_{LF},\gamma_{LF};t)\rangle \tag{14}$$

(7) While we were working on this extension and the computational methods involved, an equivalent treatment but with different emphasis appeared: Tropp, J. *J. Chem. Phys.* **1980**, *72*, 6035–6043.

(8) (a) Bolton, P. H.; James, T. L. *J. Am. Chem. Soc.* **1980**, *102*, 25–31. (b) Bolton, P. H.; James, T. L. *Biochemistry* **1980**, *19*, 1388–1392. (c) Bolton, P. H.; James, T. L. *J. Phys. Chem.* **1979**, *83*, 3359–3366. (d) Akasaka, K.; Yamada, A.; Hatano, H. *Bull. Chem. Soc. Jpn.* **1977**, *50*, 2858–2862. (e) Yamada, A.; Akasaka, K.; Hatano, H. *Biopolymers* **1978**, *17*, 749–757. (f) Tritton, T. R.; Armitage, I. M. *Nucleic Acid Res.* **1978**, *5*, 3855–3869. (g) Klevan, L.; Armitage, I. M.; Crothers, D. M. *Ibid.* **1979**, *6*, 1607–1616. (h) Davanloo, P.; Armitage, I. M.; Crothers, D. M. *Biopolymers* **1978**, *18*, 663–680. (i) Shindo, H. *Ibid.* **1980**, *19*, 509–522. (j) Shindo, H.; Wooten, J. B.; Pheiffer, B. H.; Zimmerman, S. B. *Biochemistry* **1980**, *19*, 518–526. (k) Hogan, M. E.; Jardetzky, O. *Ibid.* **1980**, *19*, 3407–3426. (l) Hogan, M. E.; Jardetzky, O. *Ibid.* **1980**, *19*, 2079–2085.

(9) (a) Spiess, H. W. *Basic Prin. Prog. NMR* **1978**, *15*, 59–214. (b) Werbelow, L. G.; Grant, D. M. *J. Chem. Phys.* **1975**, *63*, 4742–4749.

(10) Wallach, D. *J. Chem. Phys.* **1967**, *47*, 5258–5268.

$$G(\tau)_{CSA} = \left\langle \left[D_{q0}^*(\alpha_{LF},\beta_{LF},\gamma_{LF};0) + \frac{\eta}{\sqrt{6}}(D_{q2}^*(\alpha_{LF},\beta_{LF},\gamma_{LF};0) + D_{q-2}^*(\alpha_{LF},\beta_{LF},\gamma_{LF};0)) \right] \times \left[D_{q0}(\alpha_{LF},\beta_{LF},\gamma_{LF};t) + \frac{\eta}{\sqrt{6}}(D_{q2}(\alpha_{LF},\gamma_{LF},\gamma_{LF};t) + D_{q-2}(\alpha_{LF},\beta_{LF},\gamma_{LF};t)) \right] \right\rangle \quad (15)$$

The Euler angles α, β, and γ transform the F_q from the laboratory frame, L, with the z axis defined by the stationary magnetic field, to a coordinate frame, F, diagonal with the DD vector or aligned with the PAS of the CSA tensor. The asymmetry parameter, η, measures the anisotropy of the CSA tensor (eq 13). This transformation from L to F may be written as a series of transformations through intermediate coordinate frames so that each degree of motional freedom may be explicitly accounted for.[11]

$$G(\tau)_{DD} = \sum_{aa'bb'}\sum \cdots \sum_{mm'nn'}\sum \langle D_{qa}^*(\alpha_{LD},\beta_{LD},\gamma_{LD};0) \times D_{qa'}(\alpha_{LD},\beta_{LD},\gamma_{LD};t)\rangle \langle D_{ab}^*(\alpha_{D1},\beta_{D1},\gamma_{D1};0)D_{a'b'}(\alpha_{D1},\beta_{D1},\gamma_{D1};t)\rangle \cdots \langle D_{mn}^*(\alpha_{N-1,N},\beta_{N-1,N},\gamma_{N-1,N};0)D_{m'n'}(\alpha_{N-1,N},\beta_{N-1,N},\gamma_{N-1,N};t)\rangle \times \langle D_{n0}^*(\alpha_{NF},\beta_{NF},\gamma_{NF};0)D_{n'0}(\alpha_{NF},\beta_{NF},\gamma_{NF};t)\rangle \quad (16)$$

A similar expression exists for the CSA contribution, but the last ensemble average contains the D_{n+2} and D_{n-2} components (cf. eq 15). Throughout this section we will give the final transformation to a DD vector noting differences for a final transformation to a PAS of a CSA tensor as needed.

The first ensemble average represents the reorientation of an axis system, the D frame, which is embedded in the polymer. If this motion is assumed isotropic, it becomes

$$\langle D_{qa}^*(\alpha_{LD},\beta_{LD},\gamma_{LD};0)D_{qa'}(\alpha_{LD},\beta_{LD},\gamma_{LD};t)\rangle = \delta_{aa'}\tfrac{1}{5}\exp(-6D_0t) \quad (17)$$

where D_0 is the isotropic diffusion coefficient.[12]

The time-independent orientation of the first internal rotation axis with respect to the D frame does not enter the calculation because of the δ function in eq 17 and the orthogonality properties of the reduced Wigner matrices, d_{lm}.[11]

$$\sum_{bb'} d_{ab}(\beta_{D1})d_{ab'}(\beta_{D1}) = \delta_{bb'} \quad (18)$$

This means that the z axis of the D frame may be conceptualized as aligned with the first internal rotation axis. Because these two frames have a time-independent orientation with respect to one another, the first internal rotation axis also undergoes overall motion.

The overall motion may also be modeled as the anisotropic motion of a cylinder. This model is mathematically equivalent to overall isotropic motion coupled to a single free diffusion internal motion.[12]

The model chosen for internal motions determines the final form for the remaining ensemble averages in eq 16. We have used the free diffusion model and jump models between two or three nonequivalent sites for these internal motions. The free diffusion model for internal motion specifies diffusional motion about an internal rotation axis through the full 2π angular range. The jump models allow rotations about this axis through the full 2π range or any part of it in two or three discrete jumps. The final transformation to the DD vector or PAS of the CSA tensor may also make the Euler angles and the internuclear distance time dependent; consequently, we state the form for the product of

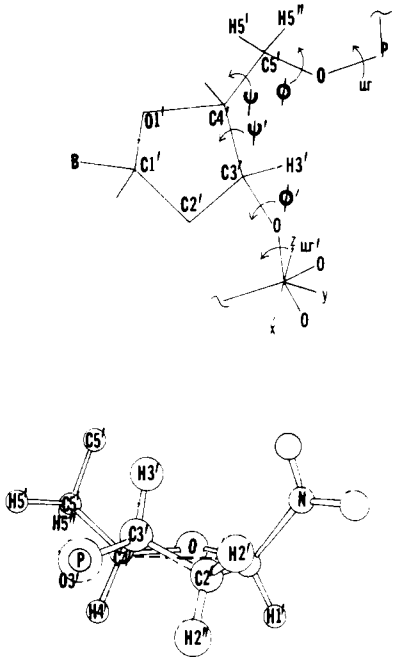

Figure 1. Definition of the DNA backbone torsion angles and the jump axis (the dashed line in the lower structure) used to define sugar repuckering. The torsion angles are defined as the clockwise rotation about B–C that aligns A–B with C–D in the sequence of atoms A–B–C–D: ω is for O3′–P–O5′–C5′; φ is for P–O5′–C5′–C4′; ψ is for O5′–C5′–C4′–C3′; ψ' is for C5′–C4′–C3′–O3′; φ' is for C4′–C3′–O3′–P; ω' is for C3′–O3′–P–O5′. The principal axis system is for the ^{31}P chemical shift tensor. The principal components were taken from ref 8i and are: σ_{11}, −76 ppm; σ_{22}, −16 ppm; σ_{33}, 103 ppm.

ensemble averages for the angular transformation to the last internal rotation axis ($N-1$ to N) and the final transformation (N to F) including the ensemble averaged internuclear distance dependence (i.e., r^3 for the DD mechanism of relaxation). The transformation to the last internal rotation axis is representative of the previous internal rotations as well. A complete evaluation of these ensemble averages is outlined in the Appendix. The well-known result where free diffusion describes the various internal rotations is shown in eq 19. D_N is the diffusion coefficient

$$G(\tau)_{DD} = \langle D_{qa}^*(\alpha_{LD},\beta_{LD},\gamma_{LD};0)D_{qa'}(\alpha_{LD},\beta_{LD},\gamma_{LD};t)\rangle \cdots \langle D_{bc}^*(\alpha_{N-1,N},\beta_{N-1,N},\gamma_{N-1,N};0)D_{b'c'}(\alpha_{N-1,N},\beta_{N-1,N},\gamma_{N-1,N};t)\rangle \times \langle D_{c0}^*(\alpha_{NF},\beta_{NF},\gamma_{NF};0)D_{c'0}(\alpha_{NF},\beta_{NF},\gamma_{NF};t)\rangle = \tfrac{1}{5}\exp(-6D_0t) \cdots |d_{bc}(\beta_{N-1,N})|^2\frac{|d_{c0}(\beta_{NF})|^2}{r^6}\exp(-c^2D_Nt) \quad (19)$$

for rotation about the Nth rotation axis. $\beta_{N-1,N}$ is the azimuthal angle between the $(N-1)$th and Nth rotation axis, and β_{NF} is the angle between the Nth rotation axis and the DD vector.

For the jump models three cases must be distinguished. In the first case, the atoms defining the DD vector are bonded to each other. The jump axis must intersect or be rigidly attached to one of the atoms. If these constrants are met, only γ need be chosen time dependent. The result for the final internal rotation and final transformation is, for this case, given in eq 20. The sum over

$$G(\tau)_{DD} = \langle D_{qa}^*(\alpha_{LD},\beta_{LD},\gamma_{LD};0)D_{qa'}(\alpha_{LD},\beta_{LD},\gamma_{LD};t)\rangle \cdots \langle D_{bc}^*(\alpha_{N-1,N},\beta_{N-1,N},\gamma_{N-1,N};0)D_{b'c'}(\alpha_{N-1,N},\beta_{N-1,N},\gamma_{N-1,N};t)\rangle \times \langle D_{c0}^*(\alpha_{NF},\beta_{NF},\gamma_{NF};0)D_{c'0}(\alpha_{NF},\beta_{NF},\gamma_{NF};t)\rangle = \frac{1}{5}\exp(-6D_0t) \cdots \sum_n \exp(-\lambda_nt)\sum_i\sum_j c_0c_n\xi_i^0\xi_j^0\xi_i^n\xi_j^n \times \exp(ic\gamma_{Ni} - ic'\gamma_{Nj})\exp(i(b-b')\alpha_{N-1,N} + i(c-c')\alpha_{NF}) \times d_{bc}(\beta_{N-1,N})d_{b'c'}(\beta_{N-1,F})\frac{d_{c0}(\beta_{NF})d_{c'0}(\beta_{NF})}{r^6} \quad (20)$$

n is for the eigenvalues, λ_n, of the transition rate matrix for jumps between the states i and j. The c's are normalization coefficients and the ξ's are elements of the associated eigenvectors.[12] This

(11) We use the convention of Rose throughout. The transformations rotate functions from one frame to another about fixed axes: Rose, M. E. "Elementary Theory of Angular Momentum"; Wiley: New York, 1957; Chapter 4.

(12) Wittebort, R. J.; Szabo, A. *J. Chem. Phys.* **1979**, *69*, 1722–1735.

Table I. B Family of DNA Helices and Torsion Angles Used with the Calculations of Model 1[a]

	τ, (deg)	D, (Å)	TL, (deg)	TW, (deg)	H, (Å)	h_p, (deg)	ω', (deg)	Φ', (deg)	ψ, (deg)	Φ, (deg)	ω, (deg)
a	41.1	−0.2	6	−5	2.9	9.7	243	185	61	176	292
b	45.0	−1.2	17	−6	3.0	6.7	241	186	73	170	287
c	32.7	2.5	−10	0	3.0	14.8	249	184	26	187	317
d	36				3.4		261	159	31	209	321

[a] Values for structures a, b, and c are taken from ref 15 while those for structure d are taken from ref 18. The torsion angles ω', Φ', ψ, Φ, ω are defined in Figure 1. τ is the winding angle; D is the distance of the base pairs from the helix axis; TL is the tilt of the base pairs defined with respect to the perpendicular to the helix axis; TW is the twist or dihedral angle the planes of the base pairs make with one another; H is the distance between base pairs along the helix axis; h_p is the height of the narrow groove. The values given by structure d are those of the standard B form of DNA.

case is applicable to ^{13}C NMR relaxation of the deoxyribose ring in DNA (Figure 1).

The second case extends present theory to include dipolar coupled nuclei which are both attached to the jump axis but separated by two or more bonds.[7] Rotation about the jump axis changes the magnitude of the internuclear distance, $|r|$, as well as β_{NF} (eq 21). The values of β and $|r|$ are explicitly calculated

$$G(\tau)_{DD} = \langle D_{qa}^*(\alpha_{LD},\beta_{LD},\gamma_{LD};0)D_{qa'}(\alpha_{LD},\beta_{LD},\gamma_{LD};t)\rangle \ldots \langle D_{bc}^*(\alpha_{N-1,N},\beta_{N-1,N},\gamma_{N-1,N};0)D_{b'c'}(\alpha_{N-1,N},\beta_{N-1,N},\gamma_{N-1,N};t)\rangle \times \langle D_{c0}^*(\alpha_{NF},\beta_{NF},\gamma_{NF};0)D_{c'0}(\alpha_{NF},\beta_{NF},\gamma_{NF};t)\rangle = \frac{1}{5}\exp(-6D_0t)\ldots\sum_n \exp(-\lambda_n t)\sum_i\sum_j c_0c_n\xi_i^0\xi_j^0\xi_i^n\xi_j^n \times \exp(ic\gamma_{Ni} - ic'\gamma_{Nj})\exp(i(b-b')\alpha_{N-1,N} + i(c-c')\alpha_{NF}) \times d_{bc}(\beta_{N-1,N})d_{b'c'}(\beta_{N-1,N})\frac{d_{c0}(\beta_{iNF})d_{c'0}(\beta_{jNF})}{r_i^3r_j^3} \quad (21)$$

for each of the configurations i and j, in addition to γ, because this rotation makes them time dependent also. This procedure is mandatory for calculating the DD contribution to ^{31}P relaxation from H3′ due to rotation about C3′–O3′ or from H5′,H5″ due to rotation about C5′–O5′ (Figure 1).

The final case does not define a particular jump or rotation axis; the orientation of the DD vector or PAS of the CSA tensor is defined with respect to an axis system, not connected with any of the atoms defining the DD vector or PAS system (i.e., the helix axis system). In this case, α, β, and $|r|$ are time dependent. The procedure is useful for treating concerted rotations of the backbone (eq 22).

$$G(\tau)_{DD} = \langle D_{qa}^*(\alpha_{LD},\beta_{LD},\gamma_{LD};0)D_{qa'}(\alpha_{LD},\beta_{LD},\gamma_{LD};t)\rangle \times \langle D_{a0}^*(\alpha_{DF},\beta_{DF},\gamma_{DF};0)D_{a'0}(\alpha_{DF},\beta_{DF},\gamma_{DF};t)\rangle = \tfrac{1}{5}\exp(-6D_0t)\sum_n \exp(-\lambda_n)\sum_i\sum_j c_0c_n\xi_i^0\xi_j^0\xi_i^n\xi_j^n \times \exp(ia\alpha_{Di} - ia\alpha_{Dj})\frac{d_{a0}(\beta_{iDF})d_{a0}(\beta_{jDF})}{r_i^3r_j^3} \quad (22)$$

For the CSA calculations the final transformation is to the PAS of this tensor (Figure 1). In this case, eq 20–22 have no dependence on $|r|$, but a final rotation γ_F which enters via the D_{n+2} and D_{n-2} components, is necessary to align the F_q with the PAS.

Motional Model 1. Jumps Referenced to the Helical Axis. The use of the helix axis as the reference system for internal motion jumps enables us to examine the effect of concerted motions on ^{31}P and ^{13}C relaxation in DNA. The D frame may be chosen with the z axis aligned with the helix axis of DNA (Figure 2). The y axis is perpendicular to this axis and to the DD vector (C–H or P–H) or the z axis of the ^{31}P PAS at time zero. A rotation β_i about the y_i axis transforms the F_q from alignment with the helix axis to the z_i axis of the DD or CSA interaction. The CSA interaction requires a final rotation, γ_i, about the new z axis to align the F_q with the PAS. Rotations about the six backbone bonds results in a new orientation of the DD vector or z axis of the PAS with respect to their original position at a later time t. To realign the F_q one must first rotate through an angle α_j about the helix axis resulting in the y_j axis perpendicular to the plane formed by the helix axis and the reoriented DD vector or z axis of the PAS. A rotation β_j about y_j realigns the F_q to the DD or PAS interaction frame. The CSA interaction again requires the final γ_j rotation about the new z axis.[14]

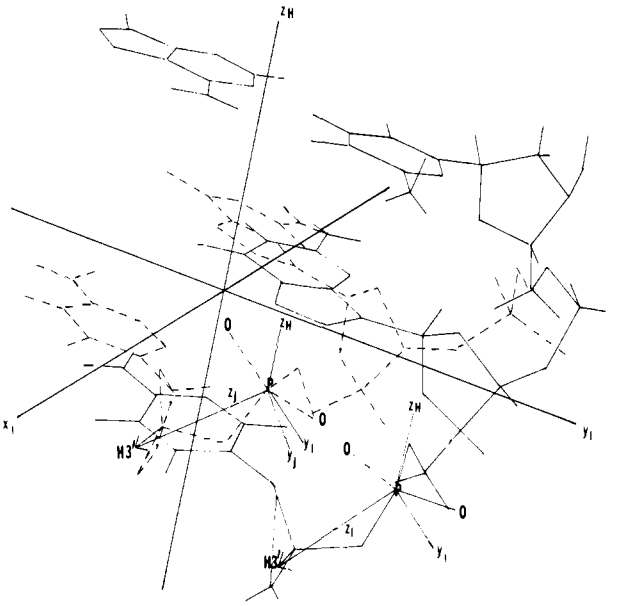

Figure 2. Reorientation of the DNA backbone by changing the torsion angles from the values listed in Table I for structure **a** (solid line) to those in structure **c** (dashed line). The z_H represents the long axis of DNA. See the text for the meaning of the other axes.

The autocorrelation function of this model (eq 22) is Fourier transformed to yield the spectral density

$$J(\omega) = \sum_{a=-2}^{2}\sum_{n=1}^{3}\sum_{i=1}^{3}\sum_{j=1}^{3}\frac{f(n)}{\omega^2 + f(n)^2}c_0c_n\xi_i^0\xi_j^0\xi_i^n\xi_j^n \times \exp(ia\alpha_{Di} - ia\alpha_{Dj})\frac{d_{a0}(\beta_{iDF})d_{a0}(\beta_{jDF})}{r_i^3r_j^3} \quad (23)$$

where,

$$f(n) = (6D_0 + \lambda_n)$$

The sums over i and j indicate that the model jumps between three states.

Although double helical DNA is found predominantly in the B form, some structural variations involving winding of the helix, tilting of the base pairs, and propeller twisting of the paired bases allow a family of energetically feasible structures to be defined.[15] Four discrete states within the B family of helices were chosen to represent the limits of the range of conformations accessible to the DNA polymer.[15] For each of these the corresponding values for the back-bone torsion angles defined in Figure 1 and the helix parameters generated by them are listed in Table I. Alternatively, Figure 3 shows the effect of a change in the torsion angles between the first and second base pairs to the values given in **a** of Table I, while keeping the torsion angles in a standard B helix, **d**, between the remaining base pairs.

In the first calculation (1-I), the three B family backbone conformational states found in the helices **a**, **b**, and **c** of Table

(13) London, R. E.; Avitabile, J. *J. Chem. Phys.* **1977**, *65*, 2443–2450.

(14) We discuss the transformations in the most conceptually convenient manner using a floating axis system. The mathematics are most conveniently treated using the convention of Rose, a fixed axis system.

(15) Zhurkin, V. B.; Lysov, Y. P.; Ivanov, V. I. *Biopolymers* **1978**, *17*, 377–412.

Table II. Internuclear Distances and Euler Angles for the Transformation from the Helix Axis System to One Aligned with the Dipole-Dipole or ^{31}P Chemical Shift Anisotropy Interaction[a]

State[a]		1				2				3			
vector	motional model[b]	α (deg)	β (deg)	γ (deg)	|r| (Å)	α (deg)	β (deg)	γ (deg)	|r| (Å)	α (deg)	β (deg)	γ (deg)	|r| (Å)
P-H3'	1-I	1.5	53.0		2.83	1.5	53.0		2.81	00	51		2.84
P-H5'	1-I	17.0	98.5		2.89	21.0	103.0		2.95	0	86		2.83
P-H5''	1-I	25.0	75.7		2.82	31.3	76.0		2.78	0	78		2.91
CSA	1-I	6.1	67.2	343.0		7.9	66.0	342.0		0	71	344	
P-H3'	1-II	0	51.5		3.01	14.8	53.1		2.83	337.3	55.8		3.01
P-H5'	1-II	0	63.9		2.69	22.2	98.6		2.89	356.2	56.1		2.69
P-H5''	1-II	0	65.2		3.09	33.2	75.8		2.82	350.7	50.7		3.10
CSA	1-II	0	75.2	322.6		355.5	67.4	306.3		358.4	80.1	307.3	
P-H3'	1-III	0	51.4		3.01	97.5	13.9		2.82				
P-H5'	1-III	0	63.9		2.69	10.8	48.2		2.90				
P-H5''	1-III	0	65.2		3.10	302.9	42.1		2.82				
CSA	1-III	0	75.2	322.6		319.3	29.7	90.6					

[a] These values are used in the calculations of model 1. [b] The three states 1, 2, and 3 are defined in the text for each of the three calculations with motional models 1-I, 1-II, and 1-III. [c] Variations in the motional models are described in the text. α, β, and γ are the Euler angles for the transformation and |r| is the magnitude of the distance separating dipolar coupled nuclei.

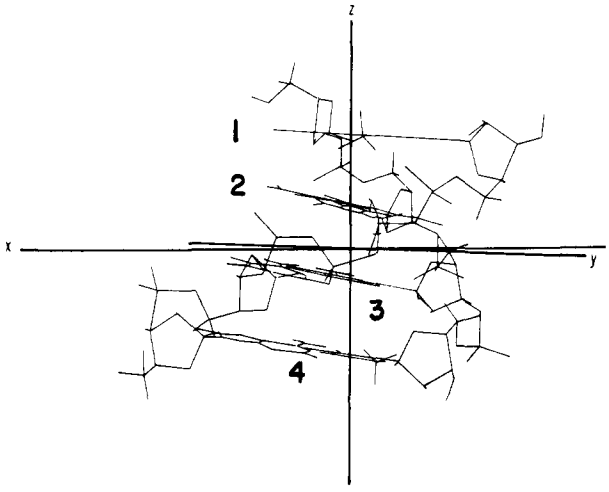

Figure 3. The reorientation of base pairs relative to the long helix axis of DNA caused by changing the torsion angles for the phosphate backbone between base pairs 1 and 2 to the values in structure **a** of Table I. The torsion angles for the phosphate backbone between base pairs 2 and 3 and base pairs 3 and 4 were kept at the values for the standard B-DNA form and are given in structure **d** of Table I.

I were used as the discrete conformations among which jumps were modeled as occurring. This three-state jump permits the DNA to jump between structures widely varying in their degree of winding and unwinding as well as base tilting and twisting. The Euler angles for the transformation from the helix axis system (frame *D*) to the ^{31}P–H DD vectors and ^{31}P PAS of helices **a**, **b**, and **c** are listed in Table II.

In the second calculation (1-II), three conformational states were also chosen. The first is state **d**, the standard B helix. The second derives from a conformational change to the torsion angles in **a**. The third conformation derives from the ^{31}P DD and PAS orientation of the ^{31}P between bases 3 and 4 given that the change in torsion angles to those in **a** occurred between bases 1 and 2 (cf. Figure 3). The Euler angles for the transformation to these conformations are listed in Table II.

In the final set of calculations using the helix axis as the frame of reference, the first backbone conformation is the standard B helix, i.e., state **d**. The second is the similar helix **a** with an additional change in sugar pucker from a phase $P = 190$ to $P = 126$.[16] The Euler angles for the two conformations used with this model, 1-III, are listed in Table II.

We have performed the analogous set of calculations for the ^{13}C atoms of the deoxyribose ring. In this case $r_i = r_j$ in eq 23.

(16) Altona, C.; Sundaralingam, M. *J. Am. Chem. Soc.* **1973**, *95*, 2333–2344.

Motional Model 2. Jumps Referenced to Rotational Axes in the Nucleotide Unit. The *D* frame is chosen with the *z* axis aligned with the jump axis which passes through C1′ or C4′ and bisecting C2′–C3′ of the deoxyribose ring (see Figure 1). Jumps about this axis result in a change of sugar pucker and provide a time-dependent reorientation of the ^{31}P DD vectors and CSA ^{31}P PAS as well as reorientation of the sugar ^{13}C DD vectors. For ^{31}P relaxation, the F_q are rotated through an angle β about the *y* axis perpendicular to the plane formed by the jump axis and the C3′–O3′ bond aligning the F_q with this bond. Rotation γ about C3′–O3′ provides a second time-dependent reorientation of the ^{31}P DD vectors and PAS. A time-independent rotation α about C3′–O3′ converts *y* to *y*′, the axis perpendicular to the plane formed by C3′–O3′ and O3′–^{31}P vectors at zero time. A rotation β about *y*′ aligns the F_q with the latter. Rotation γ about O3′–^{31}P provides the final time-dependent rotation of the PAS. A similar procedure transforms F_q from the jump axis to C5′–C4′ and then to O5′–P with C5′–O5′ dihedral angle fixed.[17] The Fourier transform of eq 21 is appropriate for this model and is given by eq 24. A similar expression gives the CSA contribution, but the

$$J(\omega) = \sum_{a=-2}^{2}\sum_{b=-2}^{2}\sum_{b'=-2}^{2}\sum_{n_1=1}^{2}\sum_{n_2=1}^{2}\sum_{i=1}^{2}\sum_{j=1}^{2}\sum_{k=1}^{2}\sum_{l=1}^{2} \frac{f(n_1n_2)}{f(n_1n_2)^2+\omega^2} \times c_0^{1}c_n^{1}\xi_i^{0}\xi_j^{0}\xi_i^{n}\xi_j^{n} \times \exp(ia(\gamma_{1i}-\gamma_{1j}))d_{ab}(\beta_{12})d_{ab'}(\beta_{12})\, c_0^{2}c_n^{2}\xi_k^{0}\xi_l^{0}\xi_k^{n}\xi_l^{n} \times \exp(ib\gamma_{2k} - ib'\gamma_{2l})\exp(i(b-b')\alpha_{2F}) \frac{d_{b0}(\beta_{k_{2F}})d_{b'0}(\beta_{l_{2F}})}{r_k^{3}r_l^{3}} \quad (24)$$

$$f(n_1n_2) = 6D_0 + \lambda_{n_1} + \lambda_{n_2}$$

summations extend over three rotations as described before. The sums over *i*, *j*, *k*, *l* indicate that each rotation was modeled as a two-state jump.

The mathematics of this model dictate that the jump axis undergoes isotropic reorientation. The internal motions occur about the jump axis and then in either the 5′–3′ or 3′–5′ direction about the intervening bonds connecting the sugar ring to phosphorus. In contrast to model 1, this model samples states involving the independent rotation of any one of the intervening bonds in addition to states derived from simultaneous rotation of several or of all them.[18]

Several calculations differing in the amplitudes allowed for the jumps about the backbone bonds were performed. In the first calculation (2-I), the limit upon $\Delta\gamma$ was picked to correspond to the rotation necessary to convert the standard B helix to the A form of DNA.[18] In the second calculation (2-II), the amplitude

(17) Rotation about O5′–P simultaneously lengthens the P–H5′ distance and shortens the P–H5′ distance. Thus we did not include this rotational degree of freedom explicitely. Φ is found near the trans position in most helices (ref 15).

(18) Arnott, S.; Campbell-Smith, P.; Chandrasekaran, R. "CRC Handbook of Biochemistry"; Vol. II; CRC Press: Cleveland, 1976; pp 411–422.

Table III. ^{31}P-H Internuclear Distances (Å) Used in Calculations for Model 2[a]

	motional model					
	2-I		2-II		2-III, 2-IV	
vector	state 1	state 2	state 1	state 2	state 1	state 2
P-H3'	3.01	2.91	3.01	2.78	3.01	2.68
P-H5'	2.70	2.70	2.70	2.70	2.70	2.70
P-H5''	3.09	3.09	3.09	3.09	3.09	3.09

[a] The distances were obtained from the program CHEM (see the Acknowledgment).

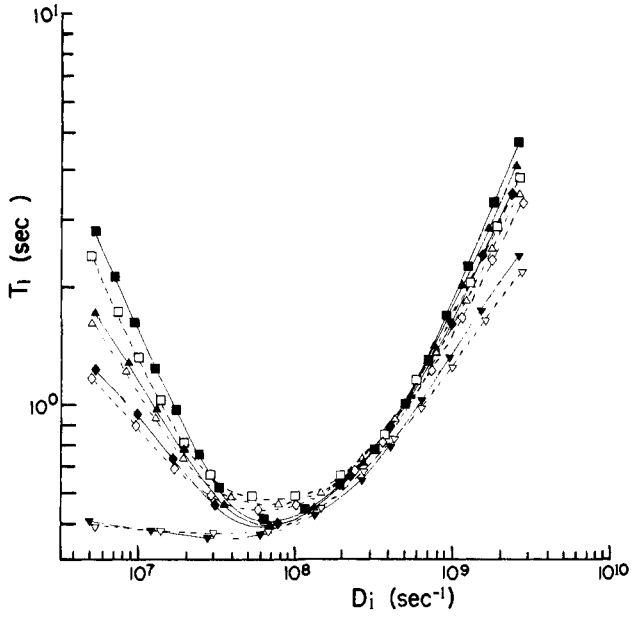

Figure 4. Comparison of ^{13}C NMR T_1 values as a function of the internal motion diffusion constant D_i for a free diffusion model (open symbols) and three-state jump model (closed symbols) in which the probabilities of each state are equal. Both calculations were performed for a single internal motion in which the ratio of the diffusion coefficient to the elementary jump rate is 5:6. Calculations were done for τ_0 values of 1000 ns (□ ■), 100 ns (△ ▲), 50 ns (◇ ◆), and 10 ns (▽ ▼). Calculations were done using a magnetic field strength of 2.35 T and a C–H bond length of 1.11 Å.

of the rotation about C3′–O3′ or C4′–C5′ was increased to 30° with the sugar repuckering remaining at ±37° as in 2-I. In the third calculation (2-III) the displacement of atoms from the mean plane of the sugar ring was restricted to ±25° with the rotation about C3′–O3′ or C4′–C5′ increasing to 50°. In the final calculation, 2-IV, rotation about the jump axis of the sugar ring was increased to ±35° with the C3′–O3′ or C4′–C5′ rotation remaining at 50°. In each of these calculations rotation about O3′–P or O5′–P was fixed at 50° because the experimental NMR data provide less information about this rotation than the others. This value was then picked as representative of rotations between the extremes found for the known helices (i.e., B-DNA and A-DNA).

The $|r|$ distances for each of the two states sampled in these four calculations are shown in Table III. The starting conformation for each calculation was the standard B helix. Again the analogous set of calculations was performed for the deoxyribose carbons.

Results

Influence of Internuclear Distances and Distance Fluctuations in NMR Relaxation. Jump models were used as a method of restricting the amplitude of internal motions in calculations of NMR relaxation parameters for DNA. Figure 4 shows a comparison of the ^{13}C T_1 values calculated assuming free diffusion and jump models using parameters designed to show that the two models may be very similar. When internal motion is very slow or very fast the differences in the two calculations have been used

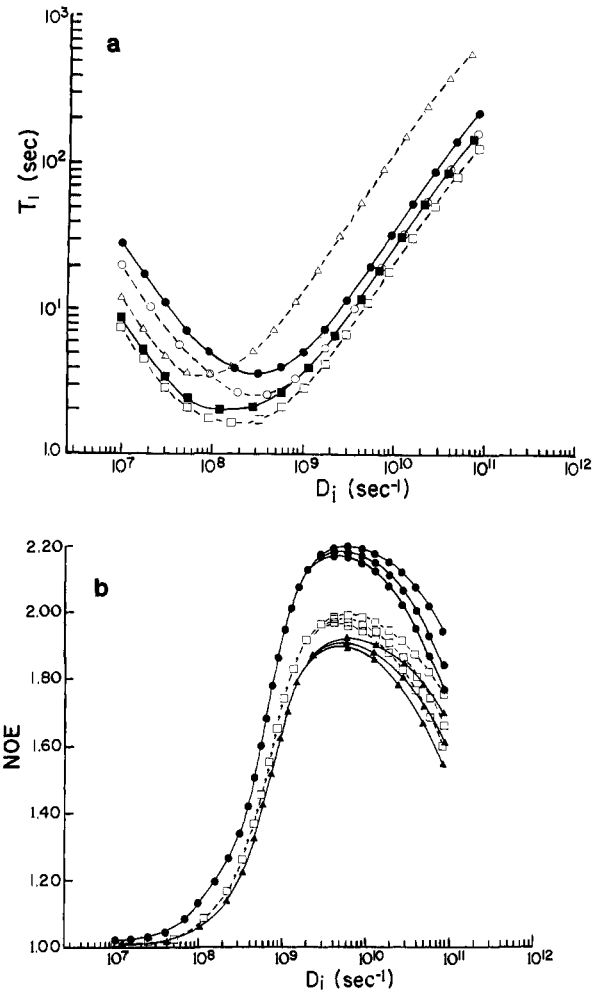

Figure 5. (a) The effect upon the ^{31}P spin–lattice relaxation time of changing the average P–H internuclear distance $|r|$ from 2.86 Å (solid symbols) to 2.7 Å (open symbols). The CSA contributon (△) which is the same in both cases is calculated using $\Delta\sigma$ = 148.5 ppm and η = −0.5825 (see ref 8i). The dipole contribution (● ○) is due to three hydrogens. The total relaxation rate (■ □) results from the CSA and DD contributions. Calculations were done at a field of 2.35 T assuming the DD and CSA interactions were modulated by an isotropic motion with correlation time τ_0 = 1000 ns and free internal diffusion with rotational diffusion coefficient D_i. (b) The effect on the calculated total NOE (1 + η) of using two different average $|r|$ distances. The solid line and circles represent the NOE assuming only dipolar contributions to ^{31}P relaxation and is independent of the distance $|r|$. The NOE values taking into account the influence of the CSA contribution to relaxation are dependent on the choice of 2.80 Å (▲) or 2.70 Å (□) for the P–H internuclear distance. Calculations were done at a field of 2.35 T assuming the DD and CSA interactions were modulated by an isotropic motion and free internal diffusion with rotatonal diffusion coefficient D_i. At the larger values of the internal diffusion constant D_i the curves for the three calculations break into three separate curves. In each type of calculation the top curve is for τ_0 = 1000 ns, the middle curve is for τ_0 = 650 ns, and the bottom curve is for τ_0 = 500 ns.

to classify the motion of a small molecule as either a jump or diffusion process.[9] The jump models have successfully treated the effect of unequally populated states upon the NMR relaxation parameters as well as identifying large amplitude motions of the appropriate frequency as most efficient in causing relaxation.[12,13] From the curves in Figure 4 it is clear that the relationship of the free diffusion model to the jump model is that of a distribution function; i.e., the T_1 curve is slightly broadened and flattened.

The ^{31}P spin–lattice relaxation time in DNA occurs in the vicinity of the T_1 minimum regardless of the model used for interpretation. Figure 5a shows the CSA and DD contribution to T_1 relaxation within the free diffusion model assuming two different average internuclear distances, r = 2.86 and 2.70 Å, for the three protons dipolar coupled to the phosphorus. The T_1

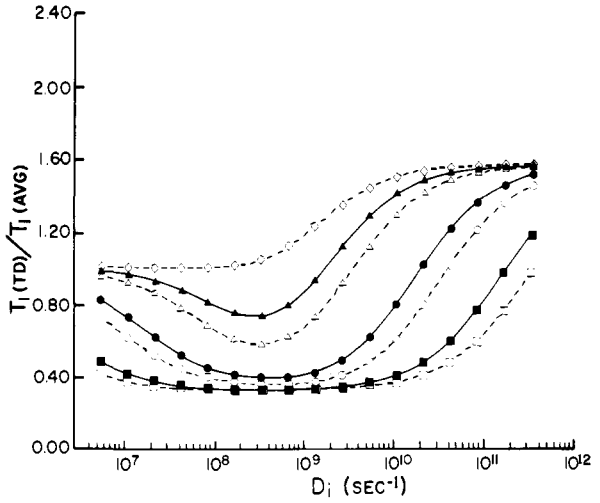

Figure 6. Ratio of proton T_1 values calculated using the explicit time-dependent internuclear distances (T_1(TD)) to the T_1 values calculated using an average value (T_1(AVG)) for the internuclear distance between the relaxing proton and the three protons on a methyl rotor which are undergoing a three-state jump. The ratio is obtained as a function of the elementary jump rate D_i. Curves are computed for τ_0 values (ns) of 1000 (□), 500 (■), 100 (○), 50 (●), 10 (△), 5 (▲), and 1 (◇).

minimum for the CSA contribution occurs at a lower frequency than that in the DD contribution, thus broadening the minimum of the total relaxation curve. A second feature of these curves is revealed by the contrast in the dipolar contribution at the two internuclear distances. At any particular given frequency of internal motion the relative DD contribution increases with the decreasing internuclear distance. While a specific T_1 may be predicted by calculations with either internuclear distance, the NOE associated with that T_1 value may be greater if the average internuclear distance is decreased. This is clearly shown by Figure 5b. If only the DD mechanism contributes to the relaxation, the NOE is independent of $|r|$ or, in other words, the strength of the interaction. If the CSA mechanism also makes a contribution, then the NOE, T_1 combination is very dependent upon $|r|$. This calculation shows that the strength of the DD interaction effected by a change in internuclear distance can be a major factor in determining the relative proportions of the CSA and DD contributions at the same amplitude of motion. This illustrates some of the consequences in assuming that the three protons H3′, H5′, and H5″ are all at the same distance from the phosphorus and do not change with motions in DNA, as we and others[8] have assumed in the past.

Figures 5a and 5b show that the proportion of the dipolar contribution also increases as the frequency of internal motion (or motions) increases and is associated with increasing T_1 values. Thus, an internal motion which decreases the average $|r|$ will give a higher NOE at a lower than expected value for T_1.

The strength of the ^{31}P–H DD coupling depends upon the amplitude of internal motion because the distance between phosphorus and the P–H3′, –H5′, and –H5″ vectors changes with the bond rotations of the backbone. We wanted to test if an average $|r|$ could be chosen to mimic the results of calculations which explicitly include changes in the magnitude of r; therefore, we performed a series of calculations on the NMR spin–lattice relaxation of a hydrogen relaxed by three methyl protons. Proton T_1 values were calculated using the spectral densities of eq 24 but for a single internal motion and explicit values of the internuclear distances in a three-state jump of the methyl rotor. For comparison, T_1 values were calculated for the same three-state jump motion using an averaged value of the internuclear distance between the relaxing protons and the three methyl protons. The averaged value was calculated from eq 25 where $p(i)$ is the

$$\langle r^{-6} \rangle = \sum_{i=1}^{n} p(i) r_i^{-6} \qquad (25)$$

equilibrium probability of the proton position in the methyl rotor.

Table IV. Experimental Relaxation Parameters for Calf Thymus DNA[a]

nucleus	T_1 (s)	$\Delta\nu_{1/2}$ (Hz)	NOE	H_0 (T)	temp (°C)
P	2.5	95	1.56	2.35	20
P	2.3	45	1.6	2.35	40
P	2.2		1.3	4.7	35
C1′, C4′	0.1		1.2	4.7	40
C2′	0.1		1.4	4.7	40
C3′	0.1		1.2	4.7	40
C5′	0.1		1.6	4.7	40

[a] Data taken from ref 8a.

Table V. Relaxation Parameters Predicted by Motional Model 1 Variants[e]

model	nucleus	T_1 (s)	$\Delta\nu_{1/2}^2$ (Hz)	NOE	%CSA	D_i^{-1},[e] (ns)
1-I	^{31}P[b]	15	37	1.22	19	6
1-II	^{31}P[b]	8	34	1.15	16	6
1-I	^{13}C[c]	1.82		1.3		8
1-III	^{31}P[b]	2.9	45	1.11	58	6

[a] $\tau_0 = 1000$ ns in all cases. Values for the principal components of the CSA tensor are taken from ref 8i and are given in the caption of Figure 1. [b] ^{31}P relaxation due to DD coupling to H3′, H5′, H5″, and to CSA at 2.35 T. [c] NT_1 is given as an average value calculated for the deoxyribose sugar ring at 4.7 T. [d] NT_1 averaged for ^{13}C deoxyribose ring atoms at 2.35 T. [e] D_i^{-1} is the inverse of the elementary jump rate.

Figure 6 shows the ratio of the T_1 value calculated using the time-dependent internuclear distances to that calculated using the average distance as a function of the jump rate D_i; the calculations were done for several values of τ_0 as shown in the various curves. In no case would the average-value calculation reproduce the explicit-distance calculation over the entire range of jump rates; in fact, the two calculations gave the same results only if the internal motion is very slow compared with overall tumbling. Various methods of obtaining an "averaged" r value met with the same result; none would lead to the same results as the more explicit calculation over the range of D_i values. Implications for DNA relaxation experiments are obvious for ^{1}H and ^{31}P NMR where rotations modulate $|r|$, but the variations in C–H distances due to vibrations are not likely to be significant.

Calculations Utilizing Motional Model 1. The experimental ^{31}P and ^{13}C relaxation data with which the calculated relaxation parameters may be compared is presented in Table IV. Since the slower motion correlation time τ_0 was determined to be about 1 μs in previous studies,[8a-c] that value was used in conjunction with the variants of the internal motion model 1 described earlier.

The values of the relaxation parameters calculated using model 1 which most closely reproduce the experimental values are listed in Table V.

Inspection of Table V reveals the inadequacy of the models 1-I and 1-II for ^{31}P and ^{13}C relaxation in the polymer. The internuclear distances (Table II) for these two models were derived from published coordinates. The minimum T_1 value (1.82 s) calculated for the ^{13}C atoms of the deoxyribose ring using model 1-I reveals that it is primarily the small angular amplitude of the motions that make these models inappropriate. We note that relative to model 1-I results, model 1-II gives a substantial reduction in the ^{31}P T_1 at the minimum despite the fact that the average internuclear distance is substantially greater. The NOE reflects this increase in the internuclear distance with a decrease in NOE, while the decrease in T_1 reveals the complexity of the relationship between the CSA and DD mechanisms.

While the four conformational states listed in Table I correspond to very different helices, variations between the four structures in the backbone DD and CSA vector with respect to the helix axis system are small. A simple way to increase the amplitude of the reorientation of the DD vector and CSA tensor is to introduce a sugar repucker of 50°. The results of the calculation using the jump model with sugar repuckering (model 1-III) are also shown

Table VI. ^{13}C Relaxation Parameters for DNA Predicted by Motional Model 2 Variants[a]

		sugar ring repucker		C4'–C5' Rotation			
model	atom	amplitude (deg)	1/jump rate (ns)	amplitude (deg)	1/jump rate (ns)	T_1 (s)	NOE
2-I	C1'	74	5			0.12	1.4
	C2'		5			0.06	1.4
	C3'		5			0.12	1.3
	C4'		5			0.12	1.3
	C5'		3	0	0	0.08	1.6
2-II	C1'	74	5			0.12	1.4
	C2'		5			0.06	1.4
	C3'		5			0.12	1.3
	C4'		5			0.12	1.4
(a)	C5'		5	30	0.1	0.10	1.4
(b)	C5'		3	30	3	0.08	1.6
2-III	C1'	50	5			0.2	1.4
	C2'		5			0.1	1.4
	C3'		6			0.2	1.3
	C4'		10			0.3	1.2
	C5'		3	50	3	0.08	1.7
2-IV	C1'	70	5			0.14	1.4
	C2'		5			0.07	1.4
	C3'		5			0.13	1.4
	C4'		5			0.18	1.4
(a)	C5'		5	50	0.4	0.10	1.7
(b)	C5'		3	50	3	0.07	1.7

[a] The calculations were done using a magnetic field strength of 4.7 and a τ_0 of 500 ns (appropriate for experimental data at 35 °C).

in Table V. The ^{31}P T_1 reaches a reasonable value, but at NOE values far reduced from the experimental, a result of the large $|r|$ distances in the calculation.

Calculations Utilizing Motional Model 2. Table VI gives the calculated values for the ^{13}C NMR relaxation parameters which most closely fit the experimental data for the several variations of model 2. The internal motion experienced by the carbon atoms (C1'–C4') in the deoxyribose ring is due entirely to jumps about the axis intersecting either C1' or C4' and bisecting C2'–C3'. Rotations about this axis result in sugar repuckering.[16] The calculation with a repuckering of 50° (model 2-III) could not be forced to fit the experimental data. An amplitude of greater than or equal to 70° for this repuckering jump (Table VI) is required to obtain a reasonable fit to the experimental ^{13}C relaxation data of Table IV within this model. In fact the C2'-endo to C3'-endo sugar repuckering corresponds to a 74° rotation about this axis in going from the B form to the A form of DNA.

Although a model which included only sugar repuckering motions was sufficient to account for the relaxation of C5', we invoked an additional rotational motion about the C4'–C5' bond in order to find a model consistent with the best model for the ^{31}P relaxation data (see the discussion below). Two procedures were used to calculate the C5' relaxation parameters. In the first procedure the jump rate of the sugar ring was fixed at 5 ns, the value found to best fit the relaxation parameters for the ring atoms. The amplitude and frequency of rotation about C4'–C5' were then varied until the relaxation parameters were approximated (calculations 2-IIa and 2-IVa of Table VI). In the second procedure, the rates of the rotations about the ring jump axis and C4'–C5' were set equal and varied simultaneously to obtain the best fits listed in Table VI (calculations 2-IIb, 2-III, and 2-IVb). Reasonable fits to the relaxation parameters could be obtained in most of the calculations utilizing the additional rotation about the C4'–C5' bond. A rotation of either 30 or 50° about C4'–C5' is sufficient to fit the data irrespective of the approach used to vary the rate of the jumps. The only requirement is that the motion be on the nanosecond time scale. Additionally, it is encouraging that the approach in which both rotations were varied simultaneously yields a value for the inverse of the jump rate D_i^{-1} not greatly inconsistent with the ring carbon calculations (i.e., 3 vs. 5 ns).

Table VII lists the ^{31}P relaxation parameters calculated using motional model 2 variants which most closely represent the experimental data. The calculations of this series differ primarily in the amplitude of the rotations about the repucker jump axis in the sugar ring and about C3'–O3'. In calculations with model 2-I, the limits of rotation about each bond corresponds to the B-DNA to A-DNA transition. This calculation does not reproduce the high ^{31}P NOE values experimentally observed at the appropriate values for T_1 because the limited 14° rotation about the C3'–O3' bond results in large P–H3' distances in both of the occupied states (Table III). Since it was apparent that puckering motions in the sugar ring were inadequate to account for the ^{31}P relaxation data, additional rotational motions in the phosphodiester moiety of DNA were considered. In calculations with model 2-II, the 30° rotation about C3'–O3', results in an increased NOE value at the appropriate T_1 by reducing the P–H3' distances in the second state to a value of 2.78 Å.

A rotation about C3'–O3' of 50° reduces this distance to 2.68 Å and is the source of the slightly increased NOE values of calculation 2-IV in comparison to 2-II. The slightly better fit of the data obtained by increasing the C3'–O3' bond rotation amplitude may be offset by decreasing the amplitude of the sugar ring pucker (cf. results of calculations using model 2-III in Table VII).

The best fit of the ^{31}P data is given by 2-IVa and compares favorably with the experimental data at both fields (Table IV). The predicted NOE values are slightly lower in comparison with the experimental values; however, this series of calculations has illuminated the factors responsible for the decrease. In the model 2 calculations, the sugar repucker jump axis was chosen as the reference axis and internal rotations occur relative to this axis in the 3'–5' direction toward the phosphorus atom. The implicit assumption in this model is that compensating rotations about P–O5' and C5'–C4' of equal amplitude to those about O3'–P and C3'–O3' occur. Calculation 2-IVa for ^{31}P relaxation then allows us to favor the ^{13}C calculations having a rotation about C4'–C5' of 50°. While the optimal fit of the ^{13}C data is obtained by fixing

Table VII. ^{31}P Relaxation Parameters for DNA Predicted by Motional Model 2 Variants[a]

model	H_0 (T)	τ_0 (ns)	D_i^{-1},[d] ns	T_1 (s)	T_{1CSA}[c] (s)	T_{1DD} (s)	%CSA	NOE	NOE (DD only)	$\Delta\nu_{1/2}$ (Hz)
2-I	2.35	1000	3	2.6	7.2	4.2	35	1.2	1.6	23
2-II	2.35	1000	3	2.4	6.3	3.8	28	1.3	1.7	29
2-III	2.35	1000	4	2.5	5.8	4.5	44	1.3	1.6	33
2-IVa	2.35	1000	2.5	2.4	6.6	3.8	37	1.4	1.8	25
	2.35	500	2.5	2.4	6.5	3.8	37	1.4	1.8	12
	4.7	1000	1.5	2.4	3.4	7.8	68	1.2	1.7	66
	4.7	500	1.2	2.4	3.4	7.8	68	1.2	1.6	66
2-IVb[b]	2.35	1000	1.6	2.4	6.9	3.6	34	1.3	1.5	25

[a] The calculations were performed for different amplitudes of rotation about the repucker jump axis, C3'-O3' and O3'-P bonds, or, alternatively, the jump axis, C4'-C5' and O5'-P bonds. These values are for the different motional models respectively: 2-I, 74°, 14°, 50°; 2-II, 74°, 30°, 50°; 2-III, 50°, 50°, 50°; 2-IV, 70°, 50°, 50°; $\tau_0 = 1000$ ns corresponds to experiments at 20°; $\tau_0 = 500$ ns corresponds to experiments at 40°. [b] Rotation about the jump axis was fixed at $D_i^{-1} = 5$ ns. The rates of rotation about C3'-O3' and O3'-P were set equal and varied simultaneously. [c] Values for the principal components of the CSA tensor and the asymmetry parameter are taken from ref 8*i* and are given in Figure 1. [d] D_i^{-1} is the inverse of the jump rate.

Table VIII. ^{31}P and ^{13}C NMR Relaxation Parameters Calculated Assuming a Free Internal Diffusion Model[a]

nucleus	H_0 (T)	τ_0 (ns)	D_i^{-1} (ns)	$6D_i^{-1}$ (ns)	T_1 (s)	T_{1CSA}[d] (s)	T_{1DD}	%CSA	NOE (DD only)	NOE	$\Delta\nu_{1/2}$ (Hz)
^{31}P[b]	2.35	1000	2.5	0.4	2.5	8.5	3.5	24	1.4	1.3	25
^{31}P[b]	2.35	500	3.3	0.6	2.3	6.9	3.4	13	1.3	1.2	12
^{31}P[b]	4.7	500	1.9	0.3	2.2	3.1	7.0	68	1.3	1.1	31
^{31}P[c]	2.35	1000	1.3	0.2	2.5	14.7	3.1	17	1.8	1.6	28
^{31}P[c]	2.35	500	1.6	0.3	2.3	12.3	2.8	18	1.6	1.5	14
^{31}P[c]	4.7	500	1.4	0.3	2.2	4.1	4.9	54	1.4	1.2	33
C3'	4.7	500	11.0	1.8	0.12			0	1.3		
C2'	4.7	500	7.5	1.2	0.06			0	1.4		
C1',C4'	4.7	500	10.0	1.6	0.14			0	1.4		
C5'	4.7	500	4.0	0.6	0.09			0	1.6		

[a] $\tau_0 = 1000$ ns correspond to experiments at 20 °C; $\tau_0 = 500$ to experiments at 40 °C. D_i is the diffusion coefficient for internal rotation. [b] Calculated assuming an average P-H internuclear distance of 2.86 Å. [c] Calculated assuming an average P-H internuclear distance of 2.70 Å. [d] The principal components of the CSA tensor were taken from ref 8i and are given in the caption of Figure 1.

Table IX. Comparison of Internal Motion Correlation Times τ_i (ns) for DNA[a]

	model 2	free diffusion[b]	free diffusion[c]	free diffusion	free diffusion	two-state jump[d]
^{31}P	0.3	0.3-0.6	0.2-0.3	0.3	0.4	0.3
^{31}C	0.5-0.8	0.5-2.0		1-6		0.2
ref	this work	this work	this work	8a-c	8g	8k

[a] τ_i is defined as $6D_i^{-1}$ where D_i is the diffusion constant or elementary jump rate. [b] See results of Tables VI–VIII with the average P-H distance of 2.86 Å. [c] See results of Tables VI–VIII with the average P-H distance of 2.70 Å. [d] The reported correlation time was calculated apparently as the inverse of D_i. The value listed here is as the correlation time defined in footnote *a*.

the jump rate of the sugar ring to a value of 2×10^8 s^{-1}, the analogous calculation 2-IVb for phosphorus does not fit as well as 2-IVa in which the jump rates about the backbone bonds are equal and varied simultaneously.

Comparison with Other Motional Models. For the purposes of comparison with our jump models we also performed calculations with free diffusion about a single internal rotation axis. The optimum results, vis-a-vis experimental data, for ^{31}P and ^{13}C are shown in Table VIII. This calculation is analogous to the standard models used to interpret the NMR relaxation data.[8] Literally interpreted, the free diffusion model requires that the reference axis is tumbling isotropically. We chose the C3′–O3′ bond for treating the phosphorus data and the sugar repucker jump axis for treating the carbon data. Diffusional rotation about these axes reorient the DD or CSA axis system. Our choices for these axes differ from others because we sought consistency with our jump model 2 for comparison. The calculations were performed using two different choices for the average of the three ^{31}P–H internuclear distances, i.e., 2.7 and 2.86 Å. The first choice is an average distance used by other workers, while the second corresponds to an average computed from the distances in calculation 2-III. Additionally we have included the internal motion contribution to the CSA interaction in a rigorous way. The results are comparable to those in the literature except for a slight shift to shorter correlation times for the internal motions. For example, we obtain internal rotation correlation times in the 0.2–0.3 ns range (cf. Table VIII) for phosphorus internal motion compared to the 0.3–0.4 ns range from the literature.[19] By comparing the total NOE with that calculated assuming only a dipolar contribution to ^{31}P relaxation, it is seen that including the CSA contribution causes much of this shift. By comparing the calculations at the two different internuclear distances, Table VIII also reveals that, as discussed before, a judicious choice of the average internuclear distance may enable a better fit of the data.

Table IX summarizes the best values for internal motion correlation times from the models presented here and from the literature. In comparison with the results of the free diffusion calculation, the ^{31}P internal motion correlation time based on motional model 2 and reported in Table IX is deceivingly similar. We therefore reemphasize that the τ_i listed for model 2 calculations account for both CSA and dipolar contributions to relaxation, fluctuations in the ^{31}P–H internuclear distances, and rotational wobbling in the phosphodiester moiety as well as sugar ring puckering, while the τ_i values from the free diffusion models used here and in the literature are for a single internal motion and assume an average P–H distance and those in the literature assume a negligible CSA contribution. The ^{13}C internal motion correlation times are also similar but shorter than those derived from the free diffusion calculation.[8a,c]

Line Width and τ_0 Values. We have not discussed the line-width data or calculations in detail. A quick glance at Tables IV, V, and VII reveals that calculated ^{31}P line widths are smaller than experimentally observed. This is a feature the present models share with those previously published. The generally accepted explanation is that chemical shift dispersion of the ^{31}P resonances broadens them beyond this natural line width. This has been discussed in some detail by Shindo[8i] and James.[3]

The recent acquisition of ^{13}C relaxation data of the deoxyribose ring in DNA has, in fact, pointed to a similar problem. A possible reason for the bad fit of the ^{13}C line-width data is the assumption that each monomeric unit is independent of the others in the polymer. A second reason could be the exclusion of contributions from additional internal motions; for example, a model which combines the motions of model 1 and model 2 might improve the fit of the calculated ^{13}C linewidth. We are currently investigating these and other possibilities theoretically and experimentally.

Obviously, we have chosen to simplify the model for overall motion by assuming an isotropic correlation time τ_0. Such an assumption appears to be quite reasonable for DNA longer than 600 Å, as discussed in detail elsewhere.[3] Although use of ^{31}P or ^{13}C line widths in a quantitative study of DNA dynamics is probably not justified, the off-resonance rotating frame spin–lattice relaxation experiment[3,8a,c] and the intensity ratio R obtained in that experiment are sensitive to slow motions. The value of τ_0 used in the present calculations, 500 or 1000 ns, was obtained from a simultaneous fit of all the relaxation data in our previous studies,[8a-c] but the experimental R value was a strong determinent of the τ_0 value. In fact, the T_1 values and NOE values change very little as τ_0 changes from 300 to 1000 ns.[8a-c]

Discussion

Our intention in this paper has been first to present a viable approach for interpreting NMR relaxation data using jump models which can easily incorporate the structural information provided by the molecular geometry of DNA. We used the jump formalism

(19) It should be noted that the correlation time for free internal diffusion is commonly obtained from the internal diffuson coefficient D_i as $1/(6D_i)$, while for a jump model, the inverse of the elementary jump rate $1/D_i$ is sometimes referred to as a correlation time.

to test two types of backbone motions in motional model 1 and model 2. Model 1 and model 2 are contrasted by the different choice for a reference axis which is subject to the overall motion on a microsecond time scale. The choice of the helix axis as the reference axis in motional model 1 facilitated the treatment of concerted rotations of the six polynucleotide backbone bonds separating adjacent bases. Concerted motions of this type represent one limit of the range of conformational fluctuations that could occur in DNA. The transitions between the various states **a** through **d** in Table I reorient the plane of the bases through a range of 27° perpendicular to the helix axis (bending deformations) and wind the bases around the helix axis through a range of 9° (torsional fluctuations). The discrete states sampled are not all inclusive but representative of the continuum of possible conformational states available to DNA. The torsional and bending fluctuations of this model are somewhat greater than the root-mean-squared values for the torsion angle (3.3–5.1°), and the bending angle (4.1°) derived from the theoretical models used to interpret the fluorescence anisotropy decay of intercalated ethidium bromide.[4,5] The torsional fluctuations contribute most to the fluorescence depolarization; however, a rapid librational wobbling of 15° within the intercalation site on a time scale of a few nanoseconds is thought to be responsible for the initial rapid decay of the fluorescence anisotropy.[4d] While the wobbling is most likely confined between two base pairs, the primary torsional and bending modes contributing to the fluorescence anisotropy decay are motions of a wavelength extending over at least several base pairs.[4,5] The calculations of model 1 may be interpreted as local conformational fluctuations of the six backbone bonds separating adjacent base pairs. As an alternative interpretation consistent with the fluorescence data, concerted rotations of the backbone bonds extended over many base pairs result in conformational transitions between the helices defined by Table I. Regardless of the interpretation, the fluctuations of this model are not large enough in amplitude to reproduce the NMR data.

The reference axis subject to the microsecond overall motion in model 2 is the jump axis intersecting either C4′ or C1′ and bisecting the C2′–C3′ bond. Rotations about this axis and about C3′–O3′ or C4′–C5′ and O3′–P or O5′–P were used to model the polynucleotide backbone rotational degrees of freedom. From our best model, 2-IV, we obtain an amplitude of 70° for rotation about the jump axis. This rotation corresponds approximately to transitions between the C2′-endo and C3′-endo states. Consistent with this model are recent semiempirical energy calculations indicating a very flexible deoxyribose ring.[20]

The amplitude of rotation about C3′–O3′ and C4′–C5′ bonds were determined primarily by the relatively large observed NOE values. In this model, rotation about C3′–O3′ reduced the P–H3′ distance, increasing the calculated NOE to a value consistent with the experimental data. In contrast with model 1, model 2 represents the other extreme of completely independent rotations for the internal motions. Also in contrast to model 1, using the jump axis as the reference axis subject to the overall motion necessitates interpreting the internal motions of this model as being localized in one monomeric unit of the biopolymer. This model provides no information regarding the propagation of these internal motions to the bases or to other nucleotide units in the polymer (i.e., whether or not the nucleotides move in a concerted fashion) because the mathematics of this model stipulate that the six polynucleotide backbone rotational motions of each nucleotide unit are independent of all other nucleotide units in the polynucleotide. Any fluctuations spanning several nucleotide units have been nonspecifically included with the overall motion.

In support of the correctness of motional model 2 as a limiting form is the fact that propagation of internal motions between nucleotide units is either of too slow a frequency or of such small amplitude that the damping of these motions by the intercalator ethidium bromide appears to be confined to a single base-paired, dinucleotide unit.[8l] Recent experiments show that an initial rapid decay of the fluorescence anisotropy of the intercalated ethidium on the time scale of many picoseconds to many nanoseconds displays a $t^{1/2}$ dependence indicating that the motion of the intercalator primarily reflects the small amplitude torsional modes propagating to it from the surrounding segments of the polynucleotide.[4,5] The motions in model 2 necessary to fit the NMR data are substantially larger in amplitude than those necessary (model 1) to reorient the bases through amplitudes comparable to the long-wavelength modes monitored by the fluorescence experiments. These considerations suggest that the large amplitude local motions governing NMR relaxation are substantially uncoupled from the longer wavelength modes which determine the fluorescence depolarization. Model 1 and model 2 motions described in this work highlight the different types of information obtained from the fluorescence and NMR experiments.

Recently, models which include a 40° rotational freedom in the torsion angles ω,ω' in a virtual bond scheme were used to reproduce the equilibrium hydrodynamic properties of DNA.[6a–d] These models were constrained to maintain stacking interactions, but not necessarily hydrogen bonding interactions. The allowable tilt of two stacked bases with respect to one another that reproduce these properties was $\leq 12°$, a value within the bounds of our models. These perturbations of the polynucleotide backbone, while small, are sufficient to reproduce the worm-like behavior of DNA. However, large, but local, rotational freedom of the polynucleotide backbone introduced by single-stranded nicks have been shown to have a minimal effect upon the equilibrium hydrodynamic properties of double stranded DNA indicating that isolated large amplitude motions could occur without affecting the hydrodynamics.[21]

Recent studies into the details of nucleic acid structure via theoretical calculations,[15,20–23] X-ray diffraction,[24–28] NMR,[27–30] and other techniques[31,32] have provided evidence of the existence of variations in DNA structure from B-DNA. Differences among some of the structures entail low-energy conformational changes, some of which are sequence dependent. These studies, in conjunction with the NMR relaxation experiments, lend strength to the notion that local conformational fluctuations exist in nucleic acids which could permit the transient existence of conformations required for the nucleic acids' biological functions.

Conclusion

We have presented models for the internal mobility of DNA which elucidate the important relationships connecting the magnetic fluctuations detected by NMR with the motional fluctuations responsible for them. In this respect we have clarified what constraints the structure of DNA puts upon the internal motions. Motional models which entail DNA winding and unwinding, base tilting, and base-pair propeller twisting motions have been shown to be quite inadequate in accounting for ^{13}C and ^{31}P relaxation of backbone nuclei in DNA. A comparison of calculated and experimental ^{31}P and ^{13}C relaxation parameters has indicated that, in particular, these internal motions must increase the strength of the ^{31}P dipolar interaction (i.e., shorten the P–H

(20) (a) Kollman, P. A.; Weiner, P. K.; Dearing, A. *Biopolymers*, submitted for publication. (b) Levitt, M.; Warshel, A. *J. Am. Chem. Soc.* **1978**, *100*, 2607–2613.

(21) Hays, J. B.; Zimm, B. H. *J. Mol. Biol.* **1970**, *48*, 297–317.
(22) Selsing, E.; Wells, R. D.; Alden, C. J.; Arnott, S. *J. Biol. Chem.* **1979**, *254*, 5417–5422.
(23) Levitt, M. *Proc. Natl. Acad. Sci. U.S.A.* **1978**, *75*, 640–644.
(24) Klug, A.; Jack, A.; Viswamitra, M. A.; Kennard, O.; Shakked, Z.; Steitz, T. A. *J. Mol. Biol.* **1979**, *131*, 669–680.
(25) Wing, R.; Drew, H.; Takano, T.; Broka, C.; Tanaka, S.; Itakura, K.; Dickerson, R. E. *Nature (London)* **1980**, *287*, 755–758.
(26) Wang, A. H.-J.; Quigley, E. J.; Kolpak, F. J.; Crawford, J. L.; van Boom, J. H.; van der Marel, G.; Rich, A. *Nature (London)* **1979**, *282*, 680–686.
(27) Yamada, A.; Kaneko, H.; Akasaka, K.; Hatano, H. *FEBS Lett.* **1978**, *93*, 16–18.
(28) Patel, D. J.; Canuel, L. l.; Pohl, F. M. *Proc. Natl. Acad. Sci. U.S.A.* **1979**, *76*, 2508–2511.
(29) Shindo, H.; Simpson, R.; Cohen, J. S. *J. Biol. Chem.* **1979**, *254*, 8125–8128.
(30) Early, T. A.; Kearns, D. R.; Burd, J. F.; Larson, J. E.; Wells, R. D. *Biochemistry* **1977**, *16*, 541–551.
(31) Pohl, F. M.; Jovin, T. M. *J. Mol. Biol.* **1972**, *67*, 375–396.
(32) Griffith, J. D. *Science* **1978**, *201*, 525–527.

distance) over those possible in the standard B-DNA geometry. We have used and extended the mathematical models used to interpret NMR relaxation data in order to develop an approach for relating the structure and structural fluctuations of DNA to the magnetic fluctuations measured by the relaxation experiments. The calculations also reveal that the ^{13}C relaxation of the deoxyribose ring carbons of DNA can be accounted for by puckering motions in the sugar ring. Interpretation of the ^{31}P relaxation data and ^{13}C relaxation data on C5′ requires large amplitude rotational wobbling about the O3′–P and O5′–P bonds and about the C4′–C5′ bond or C3′–O3′ bond in addition to the sugar puckering motions. The particular model used here entailed rotational jumps about an axis passing through C1′ or C4′ and bisecting the C2′–C3′ bond. This model and its variations are only representative of many suitable combinations of internal motions which could fit the data, but as examples, they have served to put the interpretation of the NMR data in terms of internal motions on a more quantitative basis.

Acknowledgment. This work was supported by Research Grant GM 25018 from the National Institutes of Health. Joe W. Keepers thanks the American Foundation for Pharmaceutical Education for its support. We thank the staff of the departmental Computer Graphics Laboratory (supported by the Division of Research Resources NIH, Grant RR-1081-03, principal investigator, R. Langridge) for the use of their computing and graphics facilities. We are particularly indebted to Dr. Andrew Dearing whose graphics program CHEM allowed us to generate and reproduce the rotated structures in Figures 2 and 3. We are also indebted to Dr. Paul Weiner whose graphics program AMBER generated the original B-DNA structure from published coordinates and graphically displayed them.

Appendix

In this Appendix, we outlined the evaluation of the ensemble averages of the type in eq A1[12] within the context of the jump models used here.

$$\langle D_{ab}^*(\alpha_{N-1,N},\beta_{N-1,N},\gamma_{N-1,N};0)D_{a'b'}(\alpha_{N-1,N},\beta_{N-1,N},\gamma_{N-1,N};t)\rangle \times \left\langle \frac{D_{b0}^*(\alpha_{NF},\beta_{NF},\gamma_{NF};0)}{r(0)^3}\frac{D_{b'0}(\alpha_{NF},\beta_{NF},\gamma_{NF};t)}{r(t)^3}\right\rangle \quad \text{(A1)}$$

This may be rewritten as in (A2) to show explicitly the time-dependent and time-independent components of the transformation

$$\exp(i(a-a')\alpha_{N-1,N} + i(b-b')\alpha_{NF})d_{ab}(\beta_{N-1,N})d_{a'b'}(\beta_{N-1,N}) \times \left\langle \exp(ib\gamma_N(0) - ib'\gamma_N(t))\frac{d_{b0}(\beta(0))}{r(0)^3}\frac{d_{b'0}(\beta(t))}{r(t)^3}\right\rangle \quad \text{(A2)}$$

Equation A2 has been written to correspond to case 2 of the jump models (eq 21, main text). Rotation about the $N-1,N$ bond changes both the distance, r, and the angle, β, the dipolar vector makes with this axis. To evaluate this ensemble average, we calculated the conditional probability that the rotation angle γ_j occurs at time t if at time zero the rotation angle was γ_i. Because β and $|r|$ are determined by γ, this conditional probability also governs their occurrence. Equation A2 is thus rewritten

$$\exp(i(a-a')\alpha_{N-1,N} + i(b-b')\alpha_{NF})d_{ab}(\beta_{N-1,N})d_{a'b'}(\beta_{N-1,N}) \times \sum_i\sum_j P_{eq}(\gamma_{Ni})p(\gamma_{Nj},t;\gamma_{Ni},0)\exp(ib\gamma_{Ni} - ib'\gamma_{Nj})\frac{d_{b0}(\beta_i)}{r_i^3}\frac{d_{b'0}(\beta_j)}{r_j^3} \quad \text{(A3)}$$

The conditional probabilities, $p(\gamma_j,t;\gamma_i,0)$, may be most conveniently found by the method of Wittebort and Szabo.[12] A set of decay equations is constructed for the probabilities of the states i. Written in matrix notation this becomes

$$d\vec{p}/dt = \mathbf{A}\vec{p} \quad \text{(A4)}$$

where $\mathbf{A}$ is the transition rate matrix giving the constants for the transition between states. This matrix is given in eq A5 and A6

$$\begin{bmatrix} -k_1 & k_2 & k_3 \\ \frac{k_1}{2} & -k_2 & k_3 \\ \frac{k_1}{2} & k_2 & -k_3 \end{bmatrix} \quad \text{(A5)}$$

$$\begin{bmatrix} -k_1 & k_2 \\ k_1 & -k_2 \end{bmatrix} \quad \text{(A6)}$$

for the three-state and two-state jump models, respectively. The simple substitution in (A7) converts (A4) to an eigenvalue equation (A8). The solution of this set of equations leads to the eigenvalues

$$p_i(t) = \xi_i e^{-\lambda_i t} \quad \text{(A7)}$$

$$\mathbf{A}\xi = -\lambda\xi \quad \text{(A8)}$$

and vectors given by eq A9 and A10 for the three- and two-state calculations.

$$\lambda^n = \begin{bmatrix} 0 \\ k_2 + 2k_3 \\ k_1 + k_2 \end{bmatrix}; \quad \xi^0 = \begin{bmatrix} 1 \\ \frac{k_1}{2k_2} \\ \frac{k_1}{2k_2} \end{bmatrix}; \quad \xi^1 = \begin{bmatrix} 0 \\ 1 \\ -1 \end{bmatrix}; \quad \xi^2 = \begin{bmatrix} 1 \\ \frac{-1}{2} \\ \frac{-1}{2} \end{bmatrix} \quad \text{(A9)}$$

$$\lambda^n = \begin{bmatrix} 0 \\ k_1 + k_2 \end{bmatrix}; \quad \xi^0 = \begin{bmatrix} 1 \\ \frac{k_1}{k_2} \end{bmatrix}; \quad \xi^1 = \begin{bmatrix} 1 \\ -1 \end{bmatrix} \quad \text{(A10)}$$

The rate matrix may be cast into a more efficacious form for calculating the conditional probabilities by symmetrizing the transition rate matrix.[12] The eigenvectors and normalization coefficients corresponding to this matrix are given by eq A11 and A12.

$$\xi^0 = \begin{bmatrix} 1 \\ \left[\frac{k_1}{2k_2}\right]^{1/2} \\ \left[\frac{k_1}{2k_2}\right]^{1/2} \end{bmatrix}; \quad \xi^1 = \begin{bmatrix} 0 \\ 1 \\ -1 \end{bmatrix}; \quad \xi^2 = \begin{bmatrix} 1 \\ -\left[\frac{k_2}{2k_1}\right]^{1/2} \\ -\left[\frac{k_2}{2k_1}\right]^{1/2} \end{bmatrix}$$

$$c_0 = \frac{1}{1 + (k_1/k_2)}; \quad c_1 = \frac{1}{2}; \quad c_2 = \frac{k_1/k_2}{1 + (k_1/k_2)} \quad \text{(A11)}$$

$$\xi^0 = \begin{bmatrix} 1 \\ \left[\frac{k_1}{k_2}\right]^{1/2} \end{bmatrix}; \quad \xi^1 = \begin{bmatrix} 1 \\ -\left[\frac{k_2}{k_1}\right]^{1/2} \end{bmatrix}$$

$$c_0 = \frac{1}{1 + (k_1/k_2)}; \quad c_2 = \frac{k_1/k_2}{1 + (k_1/k_2)} \quad \text{(A12)}$$

The normalization coefficients result from the two constraints upon the conditional probabilities given by eq A13. The results

$$p(j,t|i,0) = p_{eq}(i) \qquad t = \infty$$

$$p(j,t|i,0) = \delta_{ij} \qquad t = 0 \quad \text{(A13)}$$

of these transformations is the simple relation,

$$p_{eq}(i)p(j,t|i,0) = \sum_n \exp(-\lambda_n t)c_0 c_n \xi_j^{(0)}\xi_i^{(0)}\xi_j^{(n)}\xi_i^{(n)} \quad \text{(A14)}$$

Plugging this into eq A3 results in eq 21 in the main text:

$$\exp(i(a-a')\alpha_{N-1,N} + i(b-b')\alpha_{NF}) \times d_{ab}(\beta_{N-1,N})d_{a'b'}(\beta_{N-1,N})\sum_n \exp(-\lambda_n t) \times \sum_i\sum_j c_0 c_n \xi_j^0\xi_i^0\xi_j^n\xi_i^n \exp(ib\gamma_i - ib'\gamma_j)\frac{d_{b0}(\beta_{iNF})}{r_i^3}\frac{d_{b'0}(\beta_{jNF})}{r_j^3} \quad \text{(A15)}$$